CFD Verification through comparison with LDP measurements of underexpanded gas leak.

Bruno Góbi Santolin[1], Márcio Ferreira Martins[2], Ramon Silva Martins[3], Fernando Augusto Ramos[4].

[1,2,3]Laboratory for Computational Transport Phenomena (LFTC), Department of Postgraduate Studies in Mechanical Engineering, Universidade Federal do Espírito Santo (Ufes), Brazil
[4]Inovetech Engenharia e Inovação, Brazil
E-mail (Bruno Góbi Santolin[1]): bruno.santolin@edu.ufes.br

Abstract

A numerical model was performed to represent the expansion phenomenon resulting from the leakage of pressurized gases in a pipe using the Ansys Fluent 2021 R1 software. The free underexpanded jet was produced by a nozzle with an outlet diameter of $2{,}7\ mm$ operating at a stagnation pressure and temperature respectively equal to $6{,}6\ atm$ and $293\ K$, being compared with the experiment conducted by Eggins and Jackson (1974) for qualitative (visual analysis) and quantitative validation requirements (through the statistical model proposed by Hanna (1993)). After the validation of the proposed numerical model, some important results can be highlighted, such as the temperature, pressure and velocity profiles, showing important regions, such as the barrel-shaped shock and the transition limit region from Mach$\gg 1$ to Mach ≤ 1 denominated "Mach disk", other important results obtained such as a peak velocity of approximately $610\ m/s$, the Mach disk position obtained at $4.5650\ mm$, a position necessary for the correct plotting of the upstream and downstream velocity profile graphs of the Mach disk. In general, the numerical model managed to meet expectations very well, agreeing with the experiment, it had excellent results for the expected velocity profiles, obtaining maximum average error for each of the compared cases of $4{,}97\%$, $5{,}28\%$ and $8{,}85\%$ for the worst case, thus validating the proposed numerical model clearly showing the main characteristics of an underexpanded free jet so necessary for leak analysis of pressurized gases.

1. Introduction

The increasing attention to safety in industries has influenced the risk assessment process, emphasizing the importance of modeling the consequences of possible accidents and their resulting scenarios. This process is fundamental, as there are regulations, strict laws, as well as standards, such as, for example, NBR ISO/IEC 31010 2012 [1] highlights that the risk management process includes the application of logical and systematic methods to establish the context to identify, analyze, evaluate and treat the risk associated with any activity, process, function or product trying to answer, for example, what can happen and what are the consequences [1]. An experimental or numerical evaluation of this phenomenon is necessary to answer the questions pertinent to the standard. Industries that work with pressurized vessels carry out the transport of these fluids through gas pipelines, and although they are relatively safe, they are subject to some failures caused by corrosion, maintenance errors, external impacts and operator errors causing the accidental release of gases from a rupture (partial or total) or hole in the ducts [2], [3].

The problem of accidental leakage, in addition to the closure of plants and interruptions of production processes, is the exposure of humans and the environment to toxic gases and contaminants. For example, once leaked, CO_2, as an asphyxiant and a heavy gas, would accumulate in low-lying areas, posing a significant risk to life [4]. A classic example happened in 1986 when an abundant amount of CO2 released from Lake Nyos in Cameroon killed 1,700 people and several domestic animals [6]. In the same way that the leakage of other well-known gases causes damage, the most diverse, such as the leakage of ammonia in refrigerators [6], or fuel gas (CH_4) which has a high risk of explosion [7].

Given the importance of studying pressurized gas leaks, it is essential to highlight how the leak happens, emphasizing the main physical phenomena. The leak of gases at high pressures begins with the depressurization in the duct through an orifice or the total rupture of the same, thus occurring in a decompression wave where all the accumulated pressure and temperature energy will be transformed into kinetic energy (by the conservation of mass and energy) occurring to the reduction of pressure and temperature, thus increasing the speed [8]. The decompression wave will start a rapid expansion from the stagnation pressure to the ambient pressure; the flow of the expansion part is usually throttled and reaches sonic speeds, that is, with very high momentum. This flow category occurs when the ratio between the two pressures is greater than the critical value [9]. When

the ratio is more significant than five, an underexpanded jet and a Mach disk formation occur after the orifice [10], as shown in Figure 1. After expansion, the underexpanded jet with very high momentum disperses through the environment; after traveling for a certain distance, the "cloud" will lose its momentum until its concentration is neglected [11].

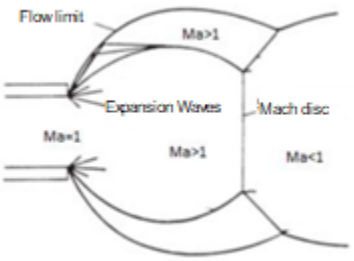

Figure 1: Structure of an underexpanded jet - Mach Disk. Adapted from (LEES, F. [12]**).**

Expanding (illustrated in Figure 1) stands out among the phenomena presented in this article. It is a very important study as it is a type of flow that involves compressibility effects, high gradients of velocity, temperature, and pressure; in addition, there is the formation of the barrel-shaped region (where Mach$\gg$ 1) [13] and the transition boundary region called "Mach disk" [14]. These sub-regions and the characteristics of the expansion phenomenon, as well as the maximum leak velocity and the Mach disk position, are parameters that are difficult to obtain precisely.

There are many challenges to the accurate modeling of the expansion phenomenon. In recent years, several works have studied the leakage phenomena, including the expansion model. The works of Wareing et al. [15] and Witlox et al. [16] adopted analytical methods that are based on the HEM model (Homogeneous Equilibrium Model), which considers that the velocity, temperature and pressure of the phases are the same and obtained consistent results, but with limitations regarding the application to pipes in smaller leak diameters [17]. Another analytical model that is widely used proposed by Bilicki and Kentin [18] and managed to meet leaks with smaller diameters was the HRM model (Homogeneous Relaxation Model), which maintained the assumption of mechanical equilibrium. Also, temperature changes are controlled by non-equilibrium effects between the liquid and vapor phases and by the metastability of liquid before evaporation. For analytical models, CFD techniques have been widely used in the studies of high-pressure gas releases due to the availability of improved computing resources. Chuech et al. [19] investigated the structure of underexpanded jets using numerical simulations and experimental methods. A version of the $k-\varepsilon$ turbulence model was proposed, introducing a compressibility correction factor for turbulent viscosity. They found that the CFD model produced encouraging results. Sand et al. [20] and Novembre et al. [21] studied accidental releases of natural gas in high-pressure pipelines. In their work, far-field dispersion was also investigated. In these studies, the fluids were modeled as ideal gases. This treatment has considerably simplified the problem but is not appropriate for correctly predicting the leakage parameters. That is because the ideal gas equation of state cannot accurately reflect the thermodynamic properties of gases at very high pressures or very low temperatures. Wareing et al. [22] and Woolley et al. [23] found that a real gas equation was considerably superior to an ideal gas equation in predicting near-field temperature and velocity profiles of jet streams. Currently, many real gas equations are available [24], [25] that can more accurately predict the vapor-liquid behavior of the flow, providing a better perspective for simulating the release of pressurized gases. Bin Liu [26] conducted a complete study of the leakage of pressurized gases through the total rupture of pipes using CFD. It is noteworthy that in the expansion model, the velocity in the profile $0{,}2\ mm$ upstream of the Mach disk was well represented; conversely, there was a discrepancy in the profiles on the axis just after the exit of the converging nozzle and $0{,}2\ mm$ downstream of the Mach disk. The experiment carried out by [27] is also highlighted, who measured the velocity fields at the jet's exit $0{,}2\ mm$ upstream and downstream of the Mach disk using the Fabry-Perot Laser-Doppler technique. This article contributes to the literature review presented by improving the numerical model for the expansion phenomenon present in the work of Bin Liu [26] in addition to the qualitative and quantitative validations (this one was not performed in the work of [26] compared to the experiment by Eggins and Jackson [27] which proved to be very accurate and a great basis for comparison for the numerical model proposed in this article.

This article aims to validade the proposed numerical model against the experiments of Eggins and Jackson [27]. Also, to generate essential data such as velocity and temperature profiles and pressure fields around the Mach disc's spatial occurence, indicating that the expansion phenomenon's main characteristics are well represented by an air underexpanded jet. Such a study is fundamental, as its results serve as a basis for further analysis of the dispersion of gases from industrial accidents involving pressurized fluids in gas pipelines.

2. Methodology

All methodology was described in this section, highlighting the numerical modeling of the expansion process of a pressurized fluid through a converging nozzle using as a basis for comparison the air jet experiment conducted by Eggins and Jackson [27] for subsequent qualitative and quantitative validation. The numerical model presented was performed using the Ansys Fluent 2021 R1 software.

In the experiment [27], high pressure air was released from a converging nozzle with an outlet diameter of 2,7 mm , stagnation pressure and temperature respectively equal to 6,6 atm and 293 K. Velocity field measurements were made using the Fabry-Perot Laser-Doppler technique. Therefore, the numerical model proposed was based on the experiment by [27].

Subsequent subsections describe the development of the geometry, mesh, equation, boundary conditions, solution methods and statistical model used for quantitative validation.

2.1 Geometry and mesh

To correctly represent the converging nozzle used in the experiment, geometry was generated in a two-dimensional domain with an axial symmetry axis represented by Figure 2 thus reducing the processing time of numerical simulations.

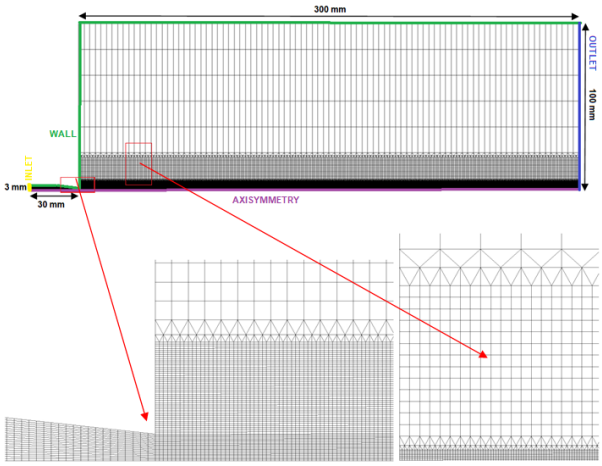

Figure 2: Geometry and mesh for the expansion model.

The domain is composed of a converging nozzle with an outlet diameter equal to 2,7 mm operating at a pressure of 6,6 atm with an outlet to the atmosphere (represented by the rectangular domain (100 mm x 300 mm)), the mesh was made aiming at better capture the behavior of the nozzle outlet to the atmosphere, so four transitions were made as shown by the zoom in Figure 2, it can be observed that the closer the nozzle is, the more refined the mesh, thus, the better use is made. of the number of elements avoiding possible indeterminacy resulting from null gradients, thus reducing the processing time of the simulations.

The preliminary mesh test was performed in order to obtain the best mesh configuration for the model following the transitions shown in the zoom of Figure 2, in addition, some preliminary tests showed that the mesh still needed a specific refinement right in the output region. , due to the high pressure and velocity gradient, as a result, an adaptive mesh was used to better capture the gradients of these variables, thus obtaining the configuration presented in Figure 3, this specific refinement resulted in a significant improvement in the results that will be shown in the section 3 totaling 104502 elements.

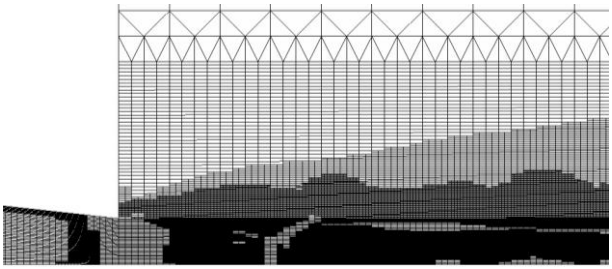

Figure 3: Adaptive mesh.

2.2 Equations for the numerical model

In the model in question was used the three conservation equations (mass, momentum and energy), $k-\varepsilon$ turbulence model, Peng Robinson's equation of state and the use of a source term in the momentum equation were used to quantify the effects of buoyancy due to the density change caused by the Peng Robson equation [28].

The mass conservation equation for a two-dimensional geometry with an axis of axial symmetry is written as follows:

$$\frac{\partial \rho}{\partial t}+\frac{\partial}{\partial x}(\rho v_x)+\frac{\partial}{\partial r}(\rho v_r)+\frac{\rho v_r}{r}=S_m \qquad (2.1)$$

Where ρ is the density of the fluid, x is the axial cordinate, r is the radial cordinate, v_x is the axial velocity, v_r is the radial velocity and S_m is the source term of the mass transferred from the continuous to the dispersed phase.

The axial and radial momentum conservation equations are given by:

$$\begin{aligned}\frac{\partial}{\partial t}(\rho v_x)+\frac{1}{r}\frac{\partial}{\partial x}(r\rho v_x v_x)+\frac{1}{r}\frac{\partial}{\partial r}(r\rho v_r v_x)=\\ -\frac{\partial p}{\partial x}+\frac{1}{r}\frac{\partial}{\partial x}\left[r\mu\left(2\frac{\partial v_x}{\partial x}-\frac{2}{3}(\nabla\cdot\vec{v})\right)\right]\\ +\frac{1}{r}\frac{\partial}{\partial r}\left[r\mu\left(\frac{\partial v_x}{\partial r}+\frac{\partial v_x}{\partial x}\right)\right]+F_x\end{aligned} \qquad (2.2)$$

and

$$\begin{aligned}\frac{\partial}{\partial t}(\rho v_r)+\frac{1}{r}\frac{\partial}{\partial x}(r\rho v_x v_r)+\frac{1}{r}\frac{\partial}{\partial r}(r\rho v_r v_r)=\\ -\frac{\partial p}{\partial r}+\frac{1}{r}\frac{\partial}{\partial x}\left[r\mu\left(\frac{\partial v_r}{\partial x}+\frac{\partial v_x}{\partial r}\right)\right]\\ +\frac{1}{r}\frac{\partial}{\partial r}\left[r\mu\left(2\frac{\partial v_r}{\partial r}-\frac{2}{3}(\nabla\cdot\vec{v})\right)\right]\\ -2\mu\frac{v_r}{r^2}+\frac{2}{3}\frac{\mu}{r}(\nabla\cdot\vec{v})+\rho\frac{{v_z}^2}{r}+F_r\end{aligned} \qquad (2.3)$$

Where, p is the static pressure, μ is the viscosity, F_x and F_r are respectively the body forces in the axial and radial direction, $(\nabla \cdot \vec{v})$ is the divergence of the velocity which is written as:

$$(\nabla \cdot \vec{v}) = \frac{\partial v_x}{\partial x} + \frac{\partial v_r}{\partial r} + \frac{v_r}{r} \tag{2.4}$$

We have that in the equation (2.3) v_z is the rotation speed given by:

$$\begin{gathered}\frac{\partial}{\partial t}(\rho v_z) + \frac{1}{r}\frac{\partial}{\partial x}(r\rho v_x v_z) \\ + \frac{1}{r}\frac{\partial}{\partial r}(r\rho v_r v_z) = \frac{1}{r}\frac{\partial}{\partial x}\left[r\mu\frac{\partial v_z}{\partial x}\right] + \\ \frac{1}{r^2}\frac{\partial}{\partial r}\left[r^3\mu\frac{\partial}{\partial r}\left(\frac{v_z}{r}\right)\right] - \rho\frac{v_r v_z}{r}\end{gathered} \tag{2.5}$$

The energy conservation equation is described as follows:

$$\begin{gathered}\frac{\partial}{\partial t}(\rho E) + \nabla \cdot \left(\vec{v}(\rho E + p)\right) = \\ \nabla \cdot \left(k_{eff}\nabla T\right) + S_{rad}\end{gathered} \tag{2.6}$$

where S_{rad} is the term radiation heat source, k_{eff} effective thermal conductivity and the energy E is given by:

$$E = h - \frac{P}{\rho} + \frac{|\vec{v}^2|}{2} \tag{2.7}$$

Where h is the enthalpy.

The turbulence model chosen was the $k-\varepsilon$ standard due to its simplicity, which is given, respectively, by the turbulent kinetic energyta k (2.8) and by dissipation ε (2.9):

$$\begin{gathered}\frac{\partial}{\partial t}(\rho k) + \frac{\partial}{\partial x_i}(\rho k u_i) = \\ \frac{\partial}{\partial x_j}\left[\frac{\mu_t}{\sigma_k}\frac{\partial k}{\partial x_j}\right] + 2\mu E_{ij}E_{ij} - \rho\varepsilon\end{gathered} \tag{2.8}$$

$$\begin{gathered}\frac{\partial}{\partial t}(\rho\varepsilon) + \frac{\partial}{\partial x_i}(\rho\varepsilon u_i) = \\ \frac{\partial}{\partial x_j}\left[\frac{\mu_t}{\sigma_\varepsilon}\frac{\partial \varepsilon}{\partial x_j}\right] + C_{1\varepsilon}\frac{\varepsilon}{k}2\mu E_{ij}E_{ij} - C_{2\varepsilon}\rho\frac{\varepsilon^2}{k}\end{gathered} \tag{2.9}$$

where u_i represents the component of velocity in the corresponding direction, E_{ij} represents the strain rate component, $\mu_t = \rho C_\mu \frac{k^2}{\varepsilon}$ represents the turbulent viscosity.

The equations (2.8) and (2.9) has adjustable constants, where their values have been obtained by numerous iterations of fitting data for a wide range of turbulent flows, and are as follows:

$$\begin{gathered}C_\mu = 0{,}09;\ \sigma_k = 1{,}00;\ \sigma_\varepsilon = 1{,}30; \\ C_{1\varepsilon} = 1{,}44;\ C_{2\varepsilon} = 1{,}92\end{gathered}$$

The equation of state must predict changes in density due to compressible flow into air, it is a constitutive equation that provides a mathematical relationship between two or more state variables associated with matter, such as its temperature, pressure, volume, or internal energy. Many different types of equation of state are used in the gas industry [29], [30] their use depends on the fluid and the phase to be analyzed to calculate its thermodynamic properties.

The ideal gas equation of state is approximately accurate for gases at low pressures and high temperatures [31], [32], however, at higher pressures and lower temperatures, such as pipeline operating conditions, it is not as effective.

The equation chosen was that of Peng Robinson, which is widely used in industrial processes, can be used for simulation in the gas phase, as it has a simple form and proven accuracy in the modeling of thermodynamic properties [33]. It is a cubic equation and is described by (2.10):

$$P = \frac{RT}{V-b} - \frac{a}{V^2 + 2bV - b^2} \tag{2.10}$$

whith:

$$a = \frac{0.45724R^2T_c^2}{P_c}\left[1 + \kappa\left(1 - \sqrt{\frac{T}{T_c}}\right)\right]^2$$

$$b = \frac{0.0778RT_c}{P_c}$$

$$\kappa = 0.37464 + 1.54226\xi - 0.26992\xi^2$$

where P is the pressure, T is the absolute temperature, V the molar specific volume, R the universal gas constant, ξ the 'acentric factor' of the gas, T_c and P_c is the temperature and pressure at the critical point, respectively.

As the density variation was adopted following the equation presented above, the effects of thrust are directly linked to this variation, as a result of which a source term was implemented for the moment equation to account for these effects and is related to the equation (2.11):

$$S = g\left(\frac{\rho_0 - \rho}{\rho}\right) \tag{2.11}$$

A UDF was made that represented the effects of buoyancy based on the equation (2.11) and compiled together with the proposed case in Ansys Fluent. The entire development of the UDF source term and its respective code is available at Appendix A.

2.3 Boundary conditions and solution methods

As boundary conditions for each of the regions shown by Figure 2 we have:

- **Inlet (Yellow line):** Prescribed temperature and pressure;
- **Wall (Green lines):** Non-slip and adiabatic;
- **Axisymmetric (purple line):** Null gradients;
- **Outlet (Blue line):** Atmospheric temperature and pressure;

Some of the considerations used were that the system is in steady state, since the stabilization of the jet occurs in approximately 40 μs [13], it was also considered that air entry and viscous forces in the expansion zone are negligible [20].

2.4 Numerical Integration

The method used in Ansys Fluent to discretize conservation equations is the finite volume method, here the computational domain is divided into a series of sub-regions called 'control volumes' or 'cells'. The governing equations are integrated over all control volumes of the computational domain. The resulting integral equations are expressed as algebraic equations that are solved numerically. [34].

The pressure-based solver was chosen because it is compatible with the two-dimensional model with axial symmetry axis used, it employs an algorithm that belongs to a general class of methods called projection method [35]. In the projection method, the mass conservation constraint of the velocity field is obtained by solving a pressure equation (or pressure correction). The pressure equation is derived from the continuity and momentum equations so that the velocity field, corrected for pressure, satisfies continuity. Since the governing equations are nonlinear and coupled to each other, the solution process involves iterations in which the entire set of governing equations is repeatedly solved until the solution converges to a proposed residue which in this case was of 10^{-4}, a summary of all solution methods used in the simulations are described in Table 1.

Table 1: Solution methods used for the simulations.

Pressure-velocity coupling		**Coupled**
Spatial discretization	Gradients	Least Squares Cell Based
	Pressure	Second order
	Density	Second order upwind
	Momentum	Second order upwind
	Turbulent kinetic energy	Second order upwind
	Turbulent dissipation rate	Second order upwind
	Energy	Second order upwind

2.5 Statistical model

For validation of the numerical model presented, it was performed in the section 3 in addition to the qualitative analysis of the results through the standard deviation of $\pm 5\%$ in the experimental results, a quantitative analysis of the experimental and numerical results was performed using the statistical method proposed by Hanna, et.al [36].

This method consists of evaluating two statistical indices that are the geometric mean (MG) and the geometric variance (VG), represented respectively by the equations (2.12) and (2.13), where C_{obs} is the value obtained in the numerical simulations and C_{exp} is the experimental value of a given parameter to be compared.

$$MG = e^{\left(ln\left(\overline{\frac{C_{obs}}{C_{exp}}}\right)\right)} \tag{2.12}$$

$$VG = e^{\left[\left(ln\left(\overline{\frac{C_{obs}}{C_{exp}}}\right)\right)^2\right]} \tag{2.13}$$

”A perfect model would have MG and VG equal to 1, while values of MG of 0,5 and 2 can be thought of as a “factor of two” over- and under-forecasts on the average, respectively” [36]. In this way, it is possible to analyze the percentage that each of the obtained indices are of factor 1, this percentage being the efficiency of the proposed numerical model.

3. Results

The recurring results in this section refer to the entire methodology presented above. First, the visual and statistical analysis of the results obtained for the velocity profile on the axis were performed. After the qualitative and quantitative validation for the axis speed, a comparison was made with the velocity profile 0,2 mm upstream and downstream of the Mach disk with their respective validations.

The results obtained for the horizontal velocity profile just after the pipe exit are shown in Figure 4 and Figure 5, it can be observed that the values obtained numerically followed the same behavior when compared to the experimental data and, in addition, the formation of the Mach disk is visible, so the physics of the problem was very well represented.

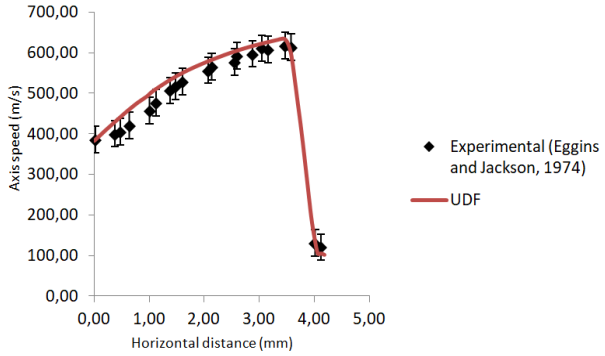

Figure 4: Axis speed.

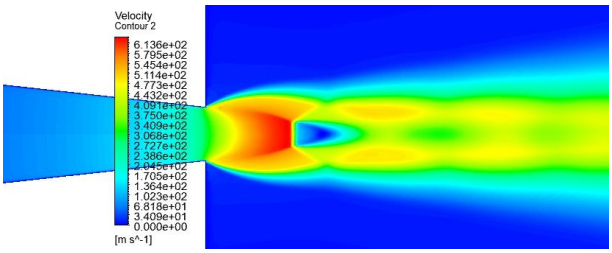

Figure 5: Speed profile.

Cheks by the Figure 4 and Figure 5 that the velocity is around 380 m/s at the exit of the tube, with a gradual increase with the distance until reaching the peak (about 610 m/s) around 3,8 mm. After that, the velocity drops significantly and then drops marginally with distance, furthermore, the formation of the barrel-shaped region where Mach $\gg 1$ [13] and also the transition boundary region called "Mach disk" [14] respecting the physics of the problem.

After the qualitative validation presented in the previous paragraphs, the quantitative analysis was also carried out through the statistical model proposed in the section 2.5. The errors obtained from the comparison of each numerical and experimental value through the parameters of the MG and VG are shown in Figure 6 and Figure 7, It is worth noting that the average error obtained for the analyzed parameters is respectively 4,968% and 0,339% , therefore, it meets the requirements for quantitative validation.

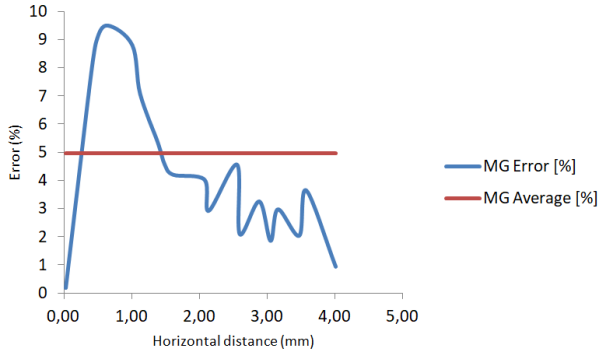

Figure 6: MG statistical parameter for axis velocity profile.

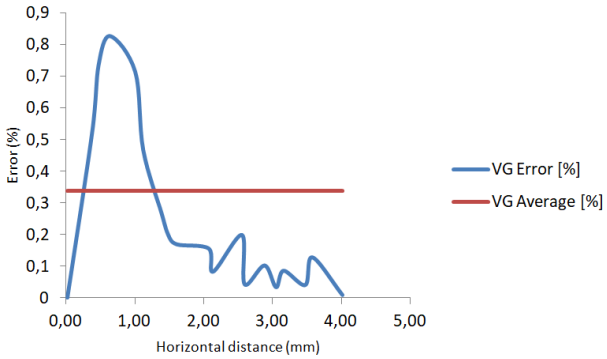

Figure 7: VG statistical parameter for axis velocity profile.

It remains to be validated for the upstream and downstream speed profiles of the Mach disk. Various profiles before and after the abrupt velocity transition were tested for later comparison purposes with the experiment conducted by [27]. After several tests, the best possible result happened at the positions of 4,33 mm and 4,8 mm respectively for the upstream and downstream velocity profiles of the Mach disk, so the position where the transition called Mach disk takes place occurs in $X_{Mach} = 4{,}565\ mm$.

According to the literature, the position where the transition occurs (X_{Mach}) is represented by the formulation proposed by Franquet, et al. [37] described by the equation (3.1), where d_{lib} is the release diameter, p_{lib} and p_{amb} are the release and ambient pressures, respectively.

$$X_{Mach} = 0{,}645 d_{lib} \sqrt{\frac{p_{lib}}{p_{amb}}} \qquad (3.1)$$

Using the results obtained by the formulation proposed by the equation (3.1) and the result obtained numerically (by averaging the positions of the profiles upstream and downstream of the Mach disk) was obtained the following values listed in Table 2, it can be observed that the values had a lag of only 2,036%, being statically equal and, therefore, within the allowed range.

Table 2: Relative error for Mach disk position.

	X_{Mach} value [mm]	Error [%]
Franquet, et al. (2015)	4,4739	0,000
Numeric	4,5650	2,036

With the validation of the numerically obtained position, the respective profiles were compared for qualitative and quantitative validation. The Figure 8 and Figure 11 show respectively the comparison of the profiles 0,2 mm upstream and downstream of the Mach disk, it can be observed that the results are well represented, having the same behavior compared to the experimental data considering a standard error of $\pm 5\%$ for each of them. The Figure 9, Figure 10, Figure 12 and Figure 13 show respectively the error behavior for each numerical value against measurements based on the parameters of MG and VG for the profiles 0,2 mm upstream and downstream of the Mach disk, the quantitative results were satisfactory, as they had an average error for each of the parameters in the respective profiles of 5,282%, 0,684%, 8,850% and 1,239%.

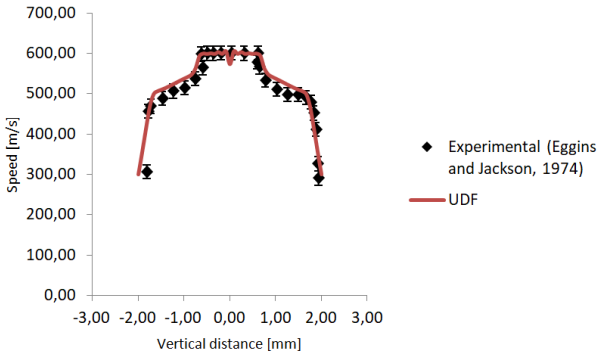

Figure 8: Velocity profile $0,2\ mm$ upstream of Mach disk.

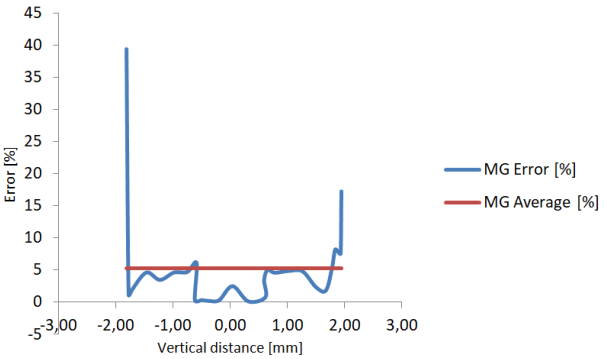

Figure 9: MG statistical parameter for velocity profile $0,2\ mm$ upstream of the Mach disk.

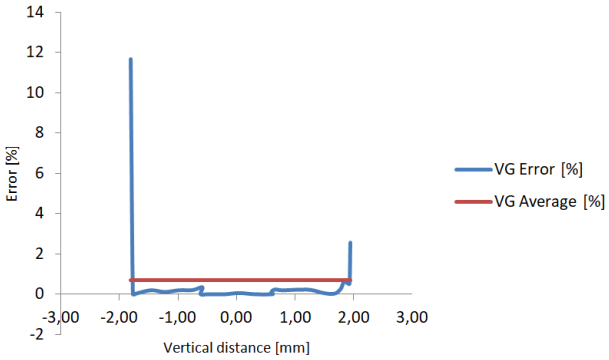

Figure 10: VG statistical parameter for velocity profile $0,2\ mm$ upstream of the Mach disk.

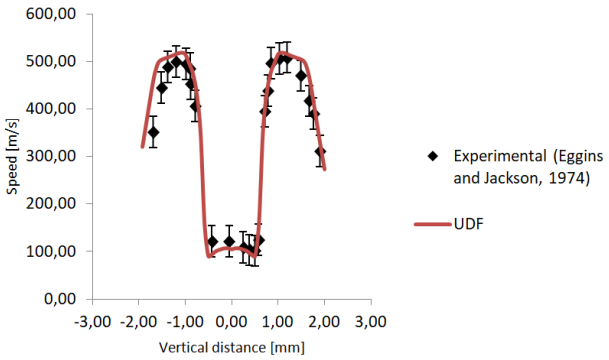

Figure 11: Velocity profile $0,2\ mm$ downstream of Mach disk.

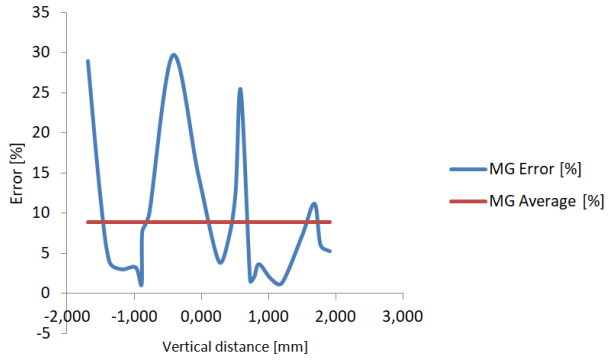

Figure 12: MG statistical parameter for velocity profile $0,2\ mm$ downstream of Mach disk.

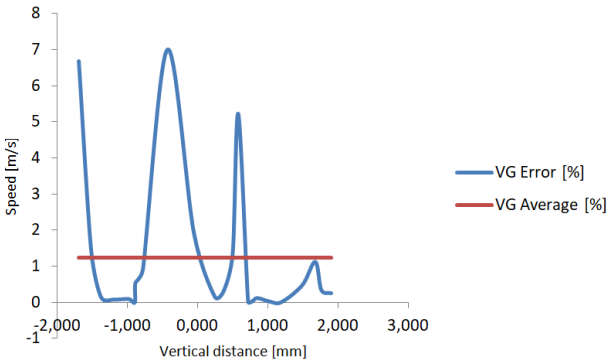

Figure 13: VG statistical parameter for velocity profile $0,2\ mm$ downstream of Mach disk.

It can be observed by Figure 8 and Figure 11 that the greatest transverse velocity occurs at the midpoint in terms of the profile $0{,}2\ mm$ upstream of the Mach disk and gradually decreases after approximately $0{,}5\ mm$, as for the profile $0{,}2\ mm$ downstream, it can be seen that the velocity is relatively low in the middle position thus respecting the physics of the problem with the barrel-shaped regions [13] and also the transition region called Mach disk [14] in addition to qualitative and quantitative validations.

Finally, observing the velocity (Figure 5), pressure (Figure 14) and temperature (Figure 15) profiles, the flow structure consists of a curved region, where the expanding flow is curved back towards the axis because of the shock with the external pressure, in this way the fully developed Mach disk can be seen. It is noticed that high speed generates low temperature due to energy conservation. The speed is maximum just a little downstream of the nozzle, while the temperature drops dramatically in this region. Downstream of the Mach disk, the velocity reduces and the temperature increases correspondingly. After the Mach disk is traversed, the speed gradually increases and the temperature tends to stabilize at room temperature.

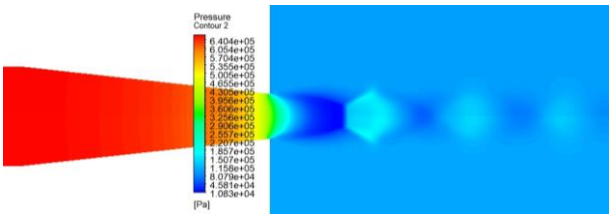

Figure 14: Pressure profile for expansion phenomenon.

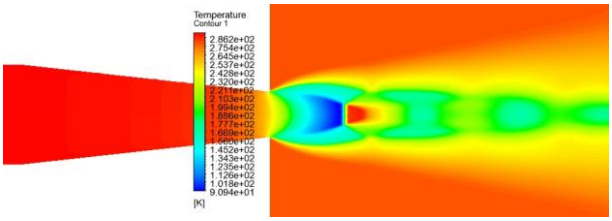

Figure 15: Temperature profile for expansion phenomenon.

4. Conclusion

This article presented a CFD model to simulate air underexpanded jets. It was found that the results obtained by the model agree well with the measurements of [27]. The preliminary mesh test allows computational time saving that after 57700 elements, there was no significant gain. Although using an adaptive mesh through the pressure and velocity gradients and implementing a UDF that accounted for the effects of buoyancy, both proved to be a satisfactory model improvements.

The model obtained excellent results, being able to recreate the main regions of the expansion phenomenon, which are the barrel shock shaped regions where Mach $\gg 1$ and also from the transition boundary region called Mach disk where Mach becomes ≤ 1 abruptly, as can be observed in the temperature, pressure and velocity profiles obtained, also showing that as a result of the leakage of pressurized gases, all the energy accumulated in the form of pressure and temperature tends to be transformed into velocity, reaching values greater than $600\ m/s$, in addition, the model was validated against the experimental data, first with the velocity profile right after the converging nozzle exit having maximum average error for the statistical parameter of the MG and VG of $4{,}968\%$ and $0{,}339\%$, after this validation the vertical velocity profiles $0{,}2\ mm$ upstream and downstream of the Mach disk were also validated with maximum mean errors respectively equal to the MG and VG of $5{,}282\%$ and $0{,}684\%$, $8{,}850\%$ and $1{,}239\%$, in addition, the position where the formation of the Mach disk occurs in $4{,}5650\ mm$ it was also validated compared to the formulation proposed by [37], an error was obtained between the values of only $2{,}036\%$, showing that the numerical model proposed in the present article is a great tool to feed the input data for gas dispersion models.

5. References

[1] (ABNT) Associação Brasileira de Normas Técnicas, *ABNT NBR ISO/IEC 31010 2012 Gestão de Riscos - Técnicas para o processo de avaliação de riscos*. Rio de Janeiro, RJ: ABNT, 2009.

[2] J. Koornneef, M. Spruijt, M. Molag, A. Ramírez, W. Turkenburg, e A. Faaij, "Quantitative risk assessment of CO2 transport by pipelines—a review of uncertainties and their impacts", *Journal of hazardous materials*, vol. 177, nº 1–3, p. 12–27, 2010.

[3] L. Teng *et al.*, "Decompression characteristics of CO2 pipelines following rupture", *Journal of Natural Gas Science and Engineering*, vol. 36, p. 213–223, 2016.

[4] K. Li, X. Zhou, R. Tu, Q. Xie, J. Yi, e X. Jiang, "An experimental investigation of supercritical CO2 accidental release from a pressurized pipeline", *The Journal of Supercritical Fluids*, vol. 107, p. 298–306, 2016.

[5] G. W. Kling *et al.*, "The 1986 lake nyos gas disaster in cameroon, west Africa", *Science*, vol. 236, nº 4798, p. 169–175, 1987.

[6] R. Purnama, S. Syafrudin, e H. Huboyo, "The Potential Impact Analysis of Ammonia Gas Leakage On Refrigeration System Using Aloha Software (Case Study At PT. Cahaya Gunung Foods)", em *IOP Conference Series: Earth and Environmental Science*, 2020, vol. 448, nº 1.

[7] D. Shindell *et al.*, "Simultaneously mitigating near-term climate change and improving human health and food security", *Science*, p. 183–189, 2012.

[8] M. Molag e C. Dam, "Modelling of accidental releases from a high pressure CO2 pipelines", *Energy Procedia*, vol. 4, p. 2301–2307, 2011.
[9] INSTITUTE, E., *Technical guidance on hazard analysis for onshore carbon capture installations and onshore pipelines.* Energy Institute, 2010.
[10] M. M. Orescanin e J. Austin, "Exhaust of underexpanded jets from finite reservoirs", *Journal of Propulsion and Power*, vol. 26, nº 4, p. 744–753, 2010.
[11] H. W. Witlox, M. Harper, A. Oke, e J. Stene, "Phast validation of discharge and atmospheric dispersion for pressurised carbon dioxide releases", *Journal of Loss Prevention in the Process Industries*, vol. 30, p. 243–255, 2014.
[12] F. Lees, *Lees' Loss prevention in the process industries: Hazard identification, assessment and control*. Butterworth-Heinemann, 2012.
[13] X. Tang, M. Asahara, A. K. Hayashi, e N. Tsuboi, "Numerical investigation of a high pressure hydrogen jet of 82 MPa with adaptive mesh refinement: The starting transient evolution and Mach disk stabilization", *international journal of hydrogen energy*, vol. 42, nº 10, p. 7120–7134, 2017.
[14] A. Abdelhamid e D. Dosanjh, "Mach disc and Riemann wave in underexpanded jet flows", em *2nd Fluid and Plasma Dynamics Conference*, 1969, p. 665.
[15] C. Wareing, M. Fairweather, S. Falle, e R. M. Woolley, "RANS modelling of sonic CO 2 jets", 2012.
[16] H. W. Witlox, M. Harper, e A. Oke, "Modelling of discharge and atmospheric dispersion for carbon dioxide releases", *Journal of Loss Prevention in the Process Industries*, vol. 22, nº 6, p. 795–802, 2009.
[17] S. Martynov, S. Brown, H. Mahgerefteh, V. Sundara, S. Chen, e Y. Zhang, "Modelling three-phase releases of carbon dioxide from high-pressure pipelines", *Process Safety and Environmental Protection*, vol. 92, nº 1, p. 36–46, 2014.
[18] Z. Bilicki e J. Kestin, "Physical aspects of the relaxation model in two-phase flow", *Proceedings of the Royal Society of London. A. Mathematical and Physical Sciences*, vol. 428, nº 1875, p. 379–397, 1990.
[19] S. Chuech, M.-C. Lai, e G. M. Faeth, "Structure of turbulent sonic underexpanded free jets", *AIAA journal*, vol. 27, nº 5, p. 549–559, 1989.
[20] I. Ø. Sand, K. Sjøen, e J. R. Bakke, "MODELLING OF RELEASE OF GAS FROM HIGH-PRESSURE PIPELINES", *International journal for numerical methods in fluids*, vol. 23, nº 9, p. 953–983, 1996.
[21] N. Novembre, F. Podenzani, e E. Colombo, "Numerical study for accidental gas releases from high pressure pipelines", 2006.
[22] C. J. Wareing, R. M. Woolley, M. Fairweather, e S. A. Falle, "A composite equation of state for the modeling of sonic carbon dioxide jets in carbon capture and storage scenarios", *AIChE Journal*, vol. 59, nº 10, p. 3928–3942, 2013.
[23] R. Woolley *et al.*, "Experimental measurement and Reynolds-averaged Navier–Stokes modelling of the near-field structure of multi-phase CO2 jet releases", *International Journal of Greenhouse Gas Control*, vol. 18, p. 139–149, 2013.
[24] H. Li e J. Yan, "Evaluating cubic equations of state for calculation of vapor–liquid equilibrium of CO2 and CO2-mixtures for CO2 capture and storage processes", *Applied Energy*, vol. 86, nº 6, p. 826–836, 2009.
[25] H. Li, J. P. Jakobsen, Ø. Wilhelmsen, e J. Yan, "PVTxy properties of CO2 mixtures relevant for CO2 capture, transport and storage: Review of available experimental data and theoretical models", *Applied Energy*, vol. 88, nº 11, p. 3567–3579, 2011.
[26] X. Liu, A. Godbole, C. Lu, B. Liu, e P. Venton, "Multi-Phase CFD Modelling of CO2 Releases From High-Pressure Pipelines", em *International Pipeline Conference*, 2016, vol. 50266, p. V002T07A009.
[27] P. Eggins e D. Jackson, "Laser-Doppler velocity measurements in an under-expanded free jet", *Journal of Physics D: Applied Physics*, vol. 7, nº 14, p. 1894, 1974.
[28] ANSYS, *ANSYS Fluent - User's Theory Guide*. Ansys, 2016.
[29] A. Cosham, R. J. Eiber, e E. B. Clark, "GASDECOM: Carbon dioxide and other components", em *International Pipeline Conference*, 2010, vol. 44212, p. 777–794.
[30] O. Kunz, R. Klimeck, W. Wagner, e M. Jaeschke, "The GERG-2004 wide-range equation of state for natural gases and other mixtures", 2007.
[31] B. E. Poling, J. M. Prausnitz, e J. P. O'connell, *Properties of gases and liquids*. McGraw-Hill Education, 2001.
[32] H. C. V. Ness, M. Abbott, M. Swihart, e J. M. Smith, *Introduction to Chemical Engineering Thermodynamics*. 2017.
[33] D.-Y. Peng e D. B. Robinson, "A new two-constant equation of state", *Industrial & Engineering Chemistry Fundamentals*, vol. 15, nº 1, p. 59–64, 1976.
[34] H. K. Versteeg e W. Malalasekera, *An Introduction to Computational Fluid Dynamics*. 2007.
[35] A. J. Chorin, "Numerical solution of the Navier-Stokes equations", *Mathematics of computation*, vol. 22, nº 104, p. 745–762, 1968.
[36] S. R. Hanna, J. Chang, e D. Strimaitis, "Hazardous gas model evaluation with field observations", *Atmospheric Environment. Part A. General Topics*, vol. 27, nº 15, p. 2265–2285, 1993.
[37] E. Franquet, V. Perrier, S. Gibout, e P. Bruel, "Free underexpanded jets in a quiescent medium: A review", *Progress in Aerospace Sciences*, vol. 77, p. 25–53, 2015.

Appendix A

Development of the UDF for a source term that accounts for the buoyancy effects due to the density change related to the Peng Robson equation:

The source term to be implemented is given by the deduction below from the radial direction moment equation only the terms related to the thrust:

$$S = -\frac{1}{\rho}\frac{\partial p}{\partial r} + F_r$$

$$S = -\frac{1}{\rho}(-\rho_0 g) - g$$

$$S = g\left(\frac{\rho_0 - \rho}{\rho}\right)$$

Deriving the above equation (2.11):

$$S = g\left(\frac{\rho_0 - \rho}{\rho}\right)$$

$$S = \left(\frac{g\rho_0 - g\rho}{\rho}\right)$$

$$S = \frac{g\rho_0}{\rho} - \frac{g\rho}{\rho}$$

$$S = g\rho_0\frac{1}{\rho} - g$$

$$\frac{dS}{d\rho} = g\rho_0\frac{d}{d\rho}\left(\frac{1}{\rho}\right) - g\frac{d}{d\rho}(1)$$

$$\frac{dS}{d\rho} = -g\rho_0\left(\frac{1}{\rho^2}\right)$$

With the source term and its respective derivative in relation to the dependent variable (ρ) the UDF was created for the source term (DEFINE_SOURCE) given by the code below:

```
#include "udf.h"

#define rho0 1.225

#define g 9.81

DEFINE_SOURCE(mom_source,c,t,dS,eqn)
{
   real source;
   source = g*(rho0-C_R(c,t))/(C_R(c,t));
   dS[eqn] = -g*rho0*(1/(C_R(c,t)*C_R(c,t)));

   return source;
}
```